Biomedical Engineering

Numerical Investigation of Three Patterns of Motion in an Electromagnetic Pulsatile VAD

Zahra Hashemi Shahraki* and Hanieh Niroomand Oscuii†

Hemolysis and thrombus formation which are critical concerns in designing a long-term implantable ventricular assist device (VAD) have impeded the widespread use of VADs. In this study, thus, the three-dimensional fluid domain of blood flow in a small bichamber positive displacement VAD (25 ml) with a magnetically levitated moving pusher plate was simulated by the means of a finite element package called ADINA. To optimize the function of the pump for minimizing shear stress induced blood damage, three different driver patterns (linear, sinusoidal, and Guyton's pulse) were investigated. The first pattern produced a constant flow, whereas the two others created pulsatile flows. The flow pattern and the distribution of shear stress of each pattern were observed for comparison. It was revealed that the three types of motions may induce less than 0.06% red blood cell damage. Moreover, in comparison to the other patterns not only did the sinusoidal motion of the pusher plate cause less risk of hemolysis, but in comparison to the linear pattern, it produced a pulsatile flow which reduced the stagnation areas in chambers, lowering the probability of thrombosis. In addition, this motion eliminates the probability of cavitations as compared with the Guyton's pulse pattern. *ASAIO Journal* 2014; 60:304–310.

Key Words: ventricular assist device, pulsatile flow, maximum shear stress, hemolysis, thrombosis

The number of people worldwide with heart failure (HF) is increasing at an alarming pace. Although nowadays heart transplant operation takes place successfully, not having enough heart donors has led to the development of ventricular assist devices (VADs) as a bridge to transplant or a final destination. Although today advanced technology is used in the implantable VADs, its success depends on the performance of the blood pumps. Research has revealed that nonpulsatile blood perfusion leads to abnormal cerebral and myocardial function.[1] Thus, designing a pump that produces pulsatile blood flow similar to a native heart is essential. The main drawback of these assist devices has been the damage exerted on blood cells. Hemolysis is one of the major blood damages caused by blood pumps.[2,3] Another major problem impeding the widespread use of VADs is thrombus formation. Hemolysis and thrombosis are known to be functions of parameters such as shear rate and exposure time.[4–6] Cavitation occurrence which may occur in transient negative pressures below the vapor pressure of blood (−713 mm Hg)[7] leading to vapor bubble formation also causes blood damage.

In addition, it was found implementing flow visualization in designing a blood pump would enhance obtaining a clear view of the fluid mechanics. The pioneer methods for flow visualization were experimental.[8,9] Lately, to reduce time and expenses spent for experiments, computational simulation[10–12] are widely used. With the aid of flow visualization, it was found that many parameters such as the geometry of pump, its constitutional elements, the position and orientation of elements,[3,13,14] the driving mechanism,[11,15] and the motion pattern of the driver[12] play an important role in lowering blood damage.

In this study, a bichamber positive displacement VAD designed based on Novacor II left ventricular assist system[16] was investigated. This pump has two similar cylindrical chambers, each of which has two ports, one inlet and one outlet, located parallel at the extreme ends of the chambers, each ending with a one way valve. The inlets of the two chambers are joined to each other from their base creating the main inlet, and the outlets have such structure as well. To implant this pump in the body, two grafts are needed. One graft attaches the bottom of the left ventricle (LV) of the heart to the main inlet, and the other joins the main outlet to the aorta. As the designed VAD acts as a helper dependent on the patient's heart disease severity, it can work with various speeds making an outflow ranging from 1 to 4.8 L/min. Solutions for the blood flow were obtained by solving the full Navier–Stokes equations for the fluid. Velocity vectors and distribution, shear stress dispersion, and nodal pressure were used to evaluate the hemodynamic aspects of the model.

Material and Methods

Governing Equations and Solution Method

The governing equations for viscous incompressible fluid flow are obtained from the principle of mass and momentum

From the *Department of Mechanical Engineering (Biomechanics Group), Islamic Azad University of Najafabad, Najafabad, Iran; and †Department of Mechanical Engineering (Biomechanics Group), Sahand University of Technology, Tabriz, Iran.

Submitted for consideration October 2012; accepted for publication in revised form January 2014.

Disclosure: The authors have no conflicts of interest to report.

Reprint Requests: Hanieh Niroomand Oscuii, Department of Mechanical Engineering (Biomechanics Group), Sahand University of Technology, Sahand New Town, PO Box 51335/1996, Tabriz, Iran. Email: niroomand@sut.ac.ir.

Copyright © 2014 by the American Society for Artificial Internal Organs

DOI: 10.1097/MAT.0000000000000051

conservation. The equations in vector notations are as follows:

$$\frac{\partial \boldsymbol{U}}{\partial t} + \nabla.(\boldsymbol{F} - \boldsymbol{G}) = 0, \tag{1}$$

where

$$\boldsymbol{U} = \begin{bmatrix} 0 \\ \rho_f \vec{v} \end{bmatrix}, \boldsymbol{F} = \begin{bmatrix} \rho_f \vec{v} \\ \rho_f \vec{v}\vec{v} \end{bmatrix}, \boldsymbol{G} = \begin{bmatrix} 0 \\ \tau \end{bmatrix}, \tag{2}$$

where $\vec{v}$ is the velocity vector, ρ_f is the fluid density which was assumed to be the density of blood, and τ is the stress tensor, which its components are given by

$$\tau_{ij} = -P\delta_{ij} + 2\mu\gamma_{ij}, \tag{3}$$

where P is the fluid pressure, δ_{ij} is Kronecker's delta, μ is the coefficient of viscosity, and the components of the strain rate tensor (γ_{ij}) are given by

$$\gamma_{ij} = \frac{v_{ij} + v_{ji}}{2}. \tag{4}$$

Utilizing the standard Galerkin finite element discretization method for Equation 1 yields the following matrix equation in symbolic form:

$$\boldsymbol{KX} = \boldsymbol{R}, \tag{5}$$

where $\boldsymbol{K}$ is the stiffness matrix, $\boldsymbol{X}$ is the vector of unknown nodal variables (velocities and pressure), and $\boldsymbol{R}$ contains the external driving forces.

Computational Model and Blood Damages Criteria

The pump investigated in this study is made up of two 25 ml identical chambers (four total valves) and a shared pusher plate in between. The electromagnet pusher plate is suspended and is directly driven by a magnetic drive obviating the need for bearings, cams, or linkages.[16] The pusher plate has a reciprocating motion. As illustrated in **Figure 1**, in half cycle 1, this plate provides active filling of blood *via* mild negative pressure for chamber 1, and at the same time, it leads to blood ejection of chamber 2 *via* mild positive pressure. In half cycle 2, chamber 1 ejects blood while chamber 2 is filled. The force applied on the pusher plate is proportional to the current and has precise controllability. The pump's stroke displacement is 13.4 mm, causing a 21 ml stroke volume. The diameter of each chamber was fixed to 46 mm. To model the effect of the pump valves, time functions were written and used at the in/out let ports of the pump to simulate the opening/closing action.

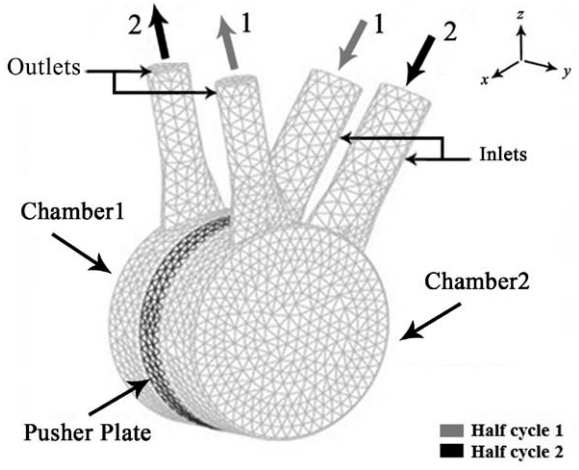

Figure 1. The geometry of the 25 ml bichamber model of pump with the pusher plate in between. The blood direction in half cycle 1 is shown with gray arrows and in half cycle 2 with black arrows.

Initially, the geometry of the blood pump was designed and then the flow field of blood in the pump was simulated. The distribution of shear stress was calculated using ADINA software (MIT, Cambridge, Massachusetts), and fluid dynamics of the blood pump were calculated at a mean pump outflow of 4.8 L/min against a pump afterload of 100 mm Hg. During the filling phase, a preload of 15 mm Hg was applied to the inflow port, whereas the outflow port was occluded. To obtain an outflow similar to the output of aorta, two different patterns were proposed: McDonald's aortic pulse and Guyton's aortic pulse (**Figure 2**).

By the means of xyExtract software (Wilton Pereira da Silva, Paraíba, Brazil) both pulses were digitized. After calculating the area under the curves, the stroke volume was achieved. By dividing it by the constant cross-section area of the inlets, the inlet velocity was calculated. By integrating the velocity *versus* time graph, the trend of the pusher plate's displacement was obtained. As illustrated in **Figure 2**, the area under the McDonald's aortic pulse is less than the one of Guyton's aortic pulse. To have the same situation, the pumps stroke displacement was set to be a constant value (13.4 mm). Thus, the total displacement was multiplied by a positive constant to reach the pumps stroke displacement. The sinusoidal motion almost fits the curve motion leading to McDonald's aortic pulse[17] (especially in the first half cycle); therefore, the sinusoidal motion was used in the simulations.

The pusher plate on the sac chamber was moved to an end-diastolic position with three different patterns: linear, sinusoidal, and the motion leading to Guyton's aortic pulse (**Figure 3**). The initial half cycle (filling phase) duration was set to 0.277 s, as it is the systole phase's duration of native hearts. As seen in **Figure 4**, almost at the end of each half cycle, all of the patterns have a change in their trend of motion; for example, from time 0 to 0.250 s, the linear pattern induces the pusher plate to move linearly with a certain slope and from time 0.250 to 0.277 s the slope of the displacement pattern changes. This will lead to the production of discrete pulses in the pump's outflow.

During the ejection phase, an afterload of 100 mm Hg was applied to the outflow port, whereas the inflow port

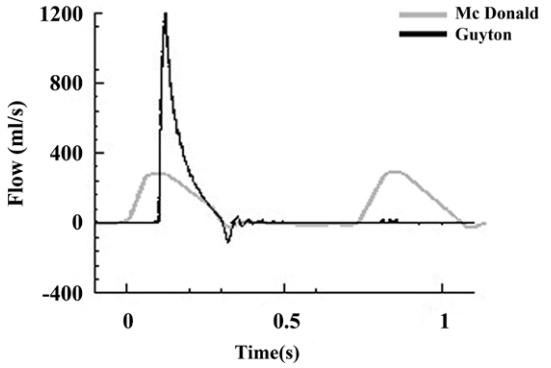

Figure 2. Mc Donald's aortic pulse[17] and Guyton's aortic pulse.[20]

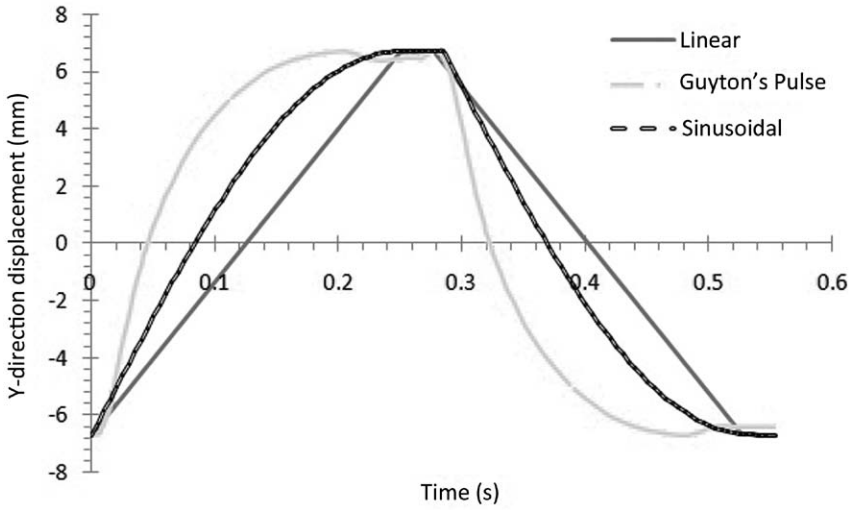

Figure 3. Displacement pattern of the actuator with time.

was occluded. The pusher plate was sent to an end-systolic position with the reverse diastolic pattern. A blood density of 1,060 kg/m^3 and a blood viscosity of 3.2×10^{-3} Pa · s were used for calculation. Finite element method analysis was run under transient and laminar flow system. Four-node tetrahedral elements with a linear interpolation function for velocity and pressure are used to discretize the fluid domain in Equation 1. Because this matrix equation is derived from the governing fluid Equation 1 and is highly nonlinear, it must be solved using an incremental iterative scheme, such as the Newton–Raphson method or the method of successive substitution within each time step. In this study, the successive method was applied.

The designed model was divided into 109,303 four-node tetrahedron elements for calculation. To attain mesh independency, five different numbers of elements (64,000, 82,000, 109,000, 150,000, and 178,000) were examined, and it was seen with about 109,000 elements that the relative error with

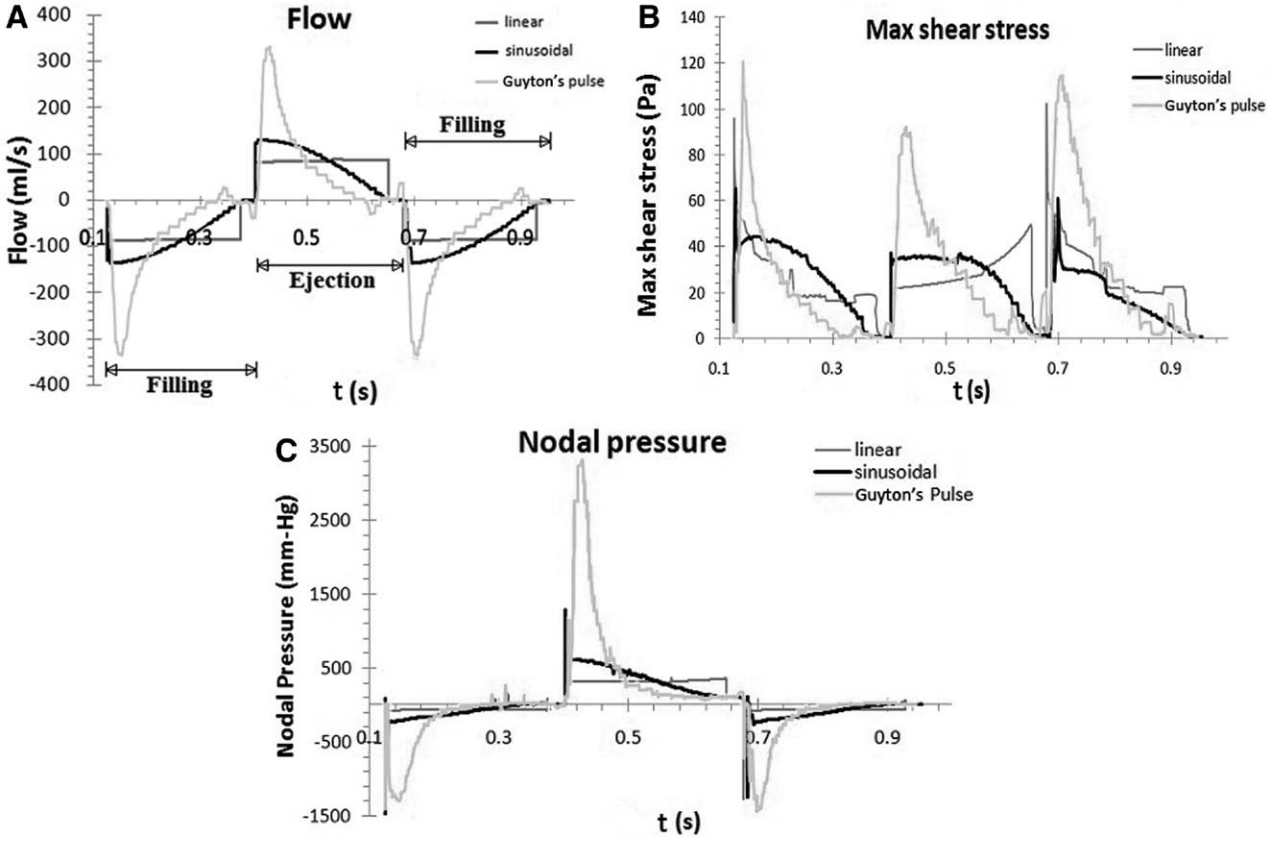

Figure 4. Results for the three patterns in chamber 2: blood flow (**A**), maximum shear stress (**B**), nodal pressure (**C**).

the higher number of elements was in the order of 10^{-4} which is a neglecting amount.

Because blood cells are viscoelastic, they can tolerate high stresses for short exposure times without hemolysis. For example, an exposure time of more than 0.1 ms at a shear stress of 1,000 Pa will produce the same amount of red cell lysis as will 150 Pa for times more than 100 s.[4] To estimate the hemolysis rate of blood cells, we applied the following mathematical correlation, which has been verified experimentally[2]:

$$L_{RBC} = \frac{dH_b}{H_b} = 3.6 \times 10^{-5}. \ \tau^{2.416}. \ t^{0.785}. \quad (6)$$

In the above equation, L_{RBC} indicates the percentage of red blood cell hemolysis, $\frac{dH_b}{H_b}$ is the ratio of the released hemoglobin in plasma to the total hemoglobin in the experimental sample, τ is the mean shear stress, and t represents the exposure time.[2,5] In this study, the whole cycle was divided into different small time steps, that is, on average 10^{-5} s. The software reported the maximum shear stress considering all the elements of each chamber for each time step. The mean maximum shear stress for each half cycle is computed by the means of MATLAB (trapezoidal numerical integration). The duration in which the mean maximum shear was taken into account is substituted for exposure time. According to Giersiepen's graph,[2] when applying the above equation, while L_{RBC} is lower than 1%, the change in the blood characteristics is venial and the blood is not in the serious damage area.[5] To reduce and prevent thrombosis formation, the stagnation areas should be reduced, and during the filling and ejection, the wall shear rate must be above 500/s.[4,6] This equals to a mean shear stress of 1.6 Pa for a blood viscosity of 3.2×10^{-3} Pa · s.

Results and Discussion

Figure 4A illustrates the blood flow within chamber 2 for all the patterns for a time period of one and a half cycles starting with the filling phase. As expected, the flow graph for each pattern is the derivative of its displacement pattern; for example, for the linear pattern, we see a constant outflow. The input and output flows of all the patterns are shown negatively and positively, respectively. Although the trend of motion of each pattern was different, its output flow was kept constant. The high peak of Guyton's aortic pulse in comparison with other flows is noticeable which is undesirable. As shown in **Figure 4A**, almost at the end of the Guyton's pulse pattern in each half cycle, during filling and ejection phases, a small retrograde flow peak followed by a small flow peak is seen. The recurrent flow correlates with the slight rise and depression in the Guyton's pattern displacement at approximately 210–240 and 490–520 ms, respectively, in each cycle (refer to **Figure 4**). The retrograde flow could be desirable for two reasons. The first reason is that in the natural heart, this opposite flow assists the valves in closing sooner,[18] and second, it could also help in blood mixing to lower thrombosis formation(Figure 8, T_3).

As shown in **Figure 4B**, for sinusoidal motion, the maximum shear stress is lower than the Guyton's aortic pulse causing less risk of hemolysis. For the linear and sinusoidal motions, the maximum shear stress among all elements by time occurs at the beginning of each filling cycle. This sudden rise in the shear stress is due to the opening of the artificial valves at the inlet port. For the Guyton's pulse, the maximum shear stress occurs at the peak of the inflow in each filling cycle. However, still among all three patterns in the worst case which is the Guyton's aortic pulse, the amount of the maximum shear stress is ultimately around 115 Pa with the exposure time of about 5×10^{-3} s resulting in 0.053% lysis which could be overlooked.

There are several serious potential problems associated with cavitation: hemolysis and thrombosis initiation, valve leaflet damage, and the formation of stable gas bubbles that may find their way to the cranial circulation. During the filling phase if the blood pressure within the chambers falls under −713 mm Hg,[7] blood may start to boil leading to cavitations in the blood chamber. **Figure 4C** shows the alteration of the nodal pressure of the central node of chamber 2 *versus* time. It is observed that the nodal pressure graph almost has the same trend of the flow graph. As seen for the Guyton's pulse, the span of variation is extremely wide and the major disadvantage of this pattern is the fall of the blood pressure within the chamber at the filling phase to an amount lower than the critical value (−1,277 mm Hg). This is due to the steep form resulted from the outflow which could raise the possibility of cavitation occurrence in the chamber. The vacuum pressures of the patterns linear and sinusoidal during the filling phase are −100 and −290 mm Hg,

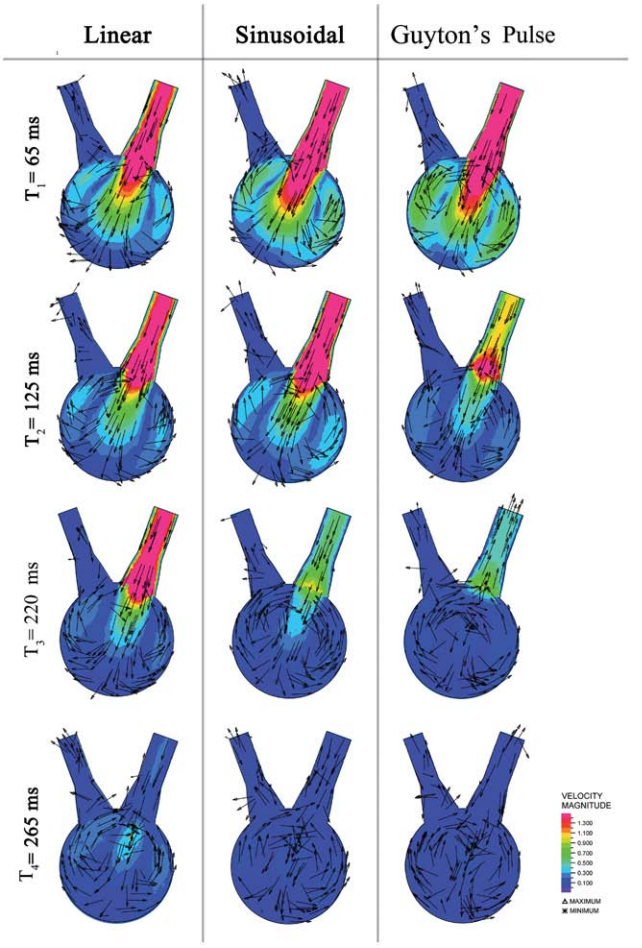

Figure 5. The velocity distribution and vectors during the filling phase in the central plane.

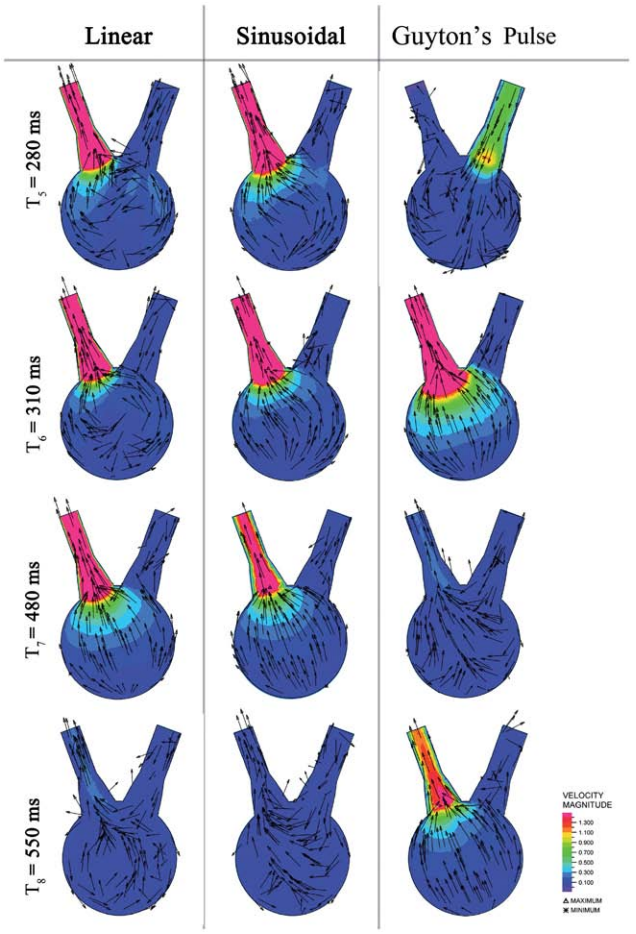

Figure 6. The velocity distribution and vectors during the ejection phase in the central plane.

respectively, which are much higher than −713 mm Hg. This quality gives these two patterns an advantage over the Guyton's pulse.

Figures 5 and 6 illustrate the velocity counters and vectors for the three patterns within chamber 2 for eight different time points (T = 65, 125, 220, 265, 280, 310, 480, and 550 ms). The results are for a cutting plane which passes through its inlet ports axis. It was revealed by rotating the ports, two vortexes were seen in the flow field within the chambers which could enhance the mixing of blood. Although in previous studies the inlet port was parallel to the outlet port, both were tangent to the chamber causing only one vortex in it.[9] **Figure 5** depicts the filling phase, as shown for the linear pattern except for the end of each half cycle (T_4), the velocity is nearly constant at T_1 and T_2, whereas for the other two patterns, the velocity variation enables blood to reach the terminal regions of the chambers which is intact for the linear pattern and reduces the possibility of thrombosis formation and blood clotting.

The velocity distribution and vectors during the systole phase are illustrated in **Figure 6**. As shown during systole and diastole phases, a region of stagnation is not observed, and for all three patterns, the blood in the chambers is dynamic. At the time the pusher plate reaches the in/outlet ports, a mild increase in the velocity is expected due to the compression of the ports which is modeled and especially seen for the linear pattern in this figure at (T_7). During the systole phase, vorticities are not observed.

As mentioned earlier, Equation 6 was used to estimate the damage exerted to blood cells. The results for two phase diastole and systole are listed in **Table 1**. To increase the reliability of the study, the results of the first half cycle in which the pump started to work was not taken into account. The results indicate that the entering blood cells do not remain in the chamber for longer than a cycle. Moreover, during the filling and ejection phase, the sinusoidal pattern has the lowest shear stress and the minimum risk of hemolysis. As shown in **Table 1**, the entire patterns act in a way that the total resulting red cell damage could be lower than 0.06% which is negligible. The LV and aortic pressure are dynamic varying between 10–120 and 80–120 mm Hg, respectively, for a native heart. For patients with HF, the maximum LV pressure and the aortic pressure decrease based on the severity of the ailment.[19] In this study, these pressures were considered static (preload = 15 mm Hg). A greater preload will lead to a better mixing and higher hemolysis risk, but as the main problem with Sac type pumps is thrombosis formation not hemolysis,[4] by underestimating the preload, the worst case of blood mixing was considered.

The shear stress distribution during the filling phase on the posterior wall of chamber 2 is shown in **Figure 7**. In the first moments of the filling phase at T_1, all the patterns, especially sinusoidal and Guyton's pulse pattern, wash the posterior wall very finely. Yet, the sinusoidal motion has more regions with wall shear rates equal to and higher than 1.6 Pa in comparison with the other patterns. During this phase, the wall shear stress decreases for all patterns. At T_2, the wall shear distribution of the linear and sinusoidal pattern is almost the same. As the jet velocity of the Guyton's pulse is higher than the other patterns, the flow will be in contact with the wall for a shorter time and spreads within the chamber faster. Thus, at T_2, Guyton's pulse has a remarkable growth in the areas with low stress (τ = 0–0.6 Pa). At T_4, for the sinusoidal and Guyton's pulse, almost stagnant regions are seen (τ = 0–0.4 Pa). They are not persistent as these areas are washed during the other parts of the cycle.

Figure 8 illustrates the ejection's phase shear stress distribution on the posterior wall of chamber 2. During this phase, except for T_8, the sinusoidal motion has lower risk of

Table 1. Results Used to Study Blood Damage

Pattern	$\overline{\tau}_{Filling}$ (Pa)	$t_{Filling}$ (s)	L_{RBC-f} (%)	$\overline{\tau}_{Ejection}$ (Pa)	$t_{Ejection}$ (s)	L_{RBC-e} (%)	$\overline{\tau}_{Total}$ (Pa)	t_{Total} (s)	L_{RBC-T} (%)
Linear	22.52	0.2768	0.0245	27.05	0.2772	0.0381	24.79	0.554	0.0582
Sinusoidal	21.86	0.2769	0.0228	26.82	0.2771	0.0374	24.34	0.554	0.0506
Guyton's pulse	25.77	0.2767	0.0339	27.12	0.2773	0.0384	26.45	0.554	0.0618

$\overline{\tau}$, the mean maximum shear stress; t, the exposure time; L_{RBC-f}:, percentage of red blood cell hemolysis during filling phase; L_{RBC-e},: percentage of red blood cell hemolysis during ejection phase; L_{RBC-T}:, the total percentage of red blood cell hemolysis in one cycle.

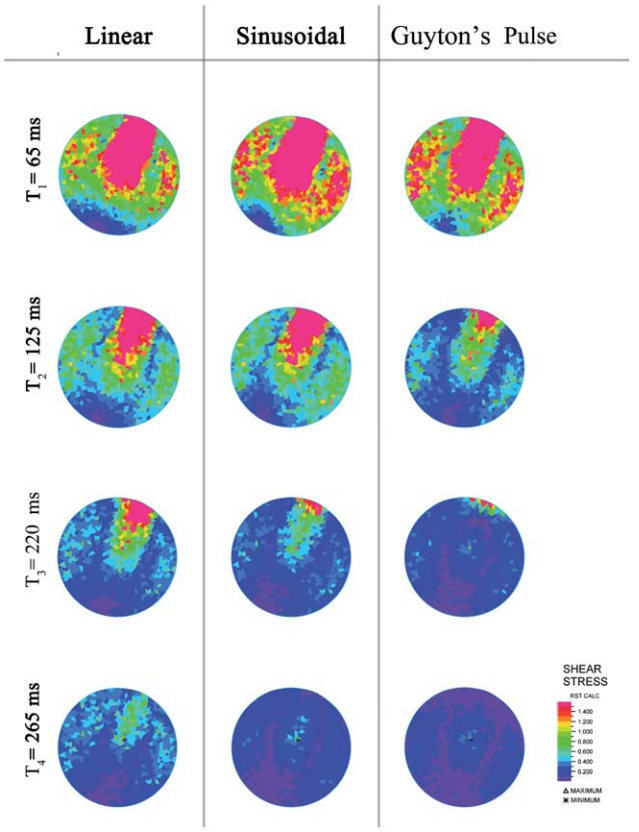

Figure 7. The shear stress distribution during the filling phase on the posterior wall.

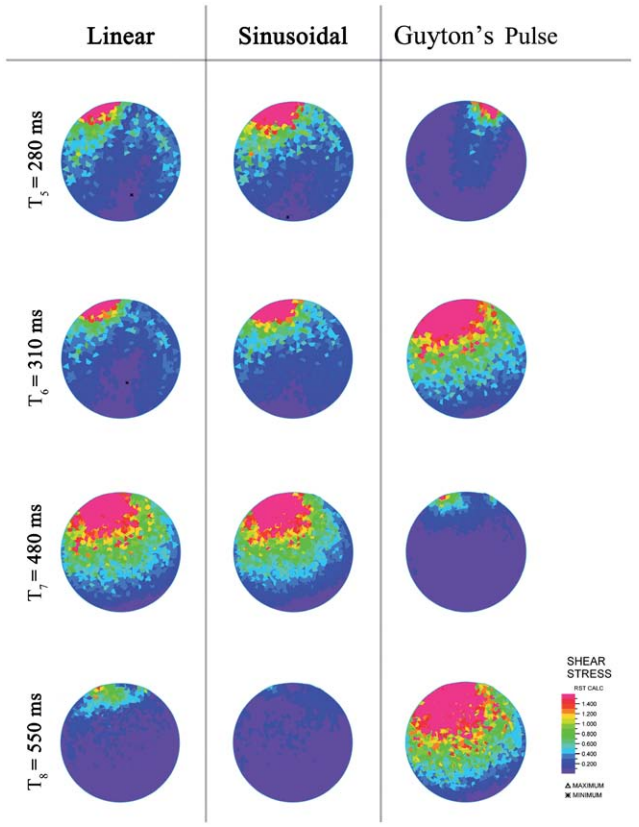

Figure 8. The shear stress distribution during the ejection phase on the posterior wall.

thrombosis in comparison with the linear motion ($\tau_{sinusoidal} \geq \tau_{linear}$). Although at T_6 and T_8 Guyton's motion leads to a better washing of the wall (wide regions with $\tau \geq 1.6$) than the other patterns, this pattern is rejected due to the probability of cavitation.

Conclusion

This study aimed to produce a pulsatile flow not only to help the patient's body to function correctly but also to minimize blood damage. Therefore, a unique small size sac type blood pump for the LV with two 25 ml identical chambers was developed. This research was the first to focus on optimizing the pusher plate's motion. Thus, three patterns of motion (linear, sinusoidal, and Guyton's pulse) were investigated. All the flows produced by the patterns cause a low amount of lysis, and for the sinusoidal motion, the time average shear stress was lower than the other patterns, causing less risk of hemolysis. In addition, by investigating velocity within the chamber and the shear stress on the wall, it was observed ultimately the three patterns almost wash all regions of the chamber. It was also revealed that stagnation regions could be reduced by increasing pulsatility and flow velocity. Thus, the Guyton's pulse and the sinusoidal pattern slightly wash the chamber better than the linear pattern. Another advantage of the sinusoidal pattern was lowering the possibility of cavitation occurrence in the filling phase compared with the Guyton's pulse. The results suggested that the sinusoidal pattern is more efficient than the other patterns investigated.

Several limitations were encountered in this study. The filling and ejection pressure of hearts was considered static not dynamic. The behavior of the in/outlet valves was simulated by time functions indicating their opening and closure, which could have been better to simulate them with actual valve models. For each heartbeat, the pump ejects three times and solely the first pulse in each cycle is superposed with a patient's heart output. Thus, using this VAD for HF cases could produce about 217 ppm. Further studies are needed to overcome these shortcomings, and it is suggested to investigate the Mc Donald's aortic pulse or even a modified version of it with increased pulsatility.

References

1. Hornick P, Taylor K: Pulsatile and nonpulsatile perfusion: The continuing controversy. *J Cardiothorac Vasc Anesth* 11: 310–315, 1997.
2. Giersiepen M, Wurzinger LJ, Opitz R, Reul H: Estimation of shear stress-related blood damage in heart valve prostheses–in vitro comparison of 25 aortic valves. *Int J Artif Organs* 13: 300–306, 1990.
3. Okamoto E, Hashimoto T, Inoue T, Mitamura Y: Blood compatible design of a pulsatile blood pump using computational fluid dynamics and computer-aided design and manufacturing technology. *Artif Organs* 27: 61–67, 2003.
4. Deutsch S, Tarbell JM, Manning KB, Rosenberg G, Fontaine AA: Experimental fluid mechanics of pulsatile artificial blood pumps. *Annu Rev Fluid Mech* 38: 65–86, 2006.
5. Bronzino JD: *The Biomedical Engineering Handbook*. Second edition. Boca Raton, FL: CRC Press LLC, 2000.
6. Fraser KH, Zhang T, Taskin ME, Griffith BP, Wu ZJ: Computational fluid dynamics analysis of thrombosis potential in left

ventricular assist device drainage cannulae. *ASAIO J* 56: 157–163, 2010.
7. Dexter EU, Aluri S, Radcliffe RR, et al: In vivo demonstration of cavitation potential of a mechanical heart valve. *ASAIO J* 45: 436–441, 1999.
8. Phillips WM, Furkay SS, Pierce WS: Laser Doppler anemometer studies in unsteady ventricular flows. *Trans Am Soc Artif Intern Organs* 25: 56–60, 1979.
9. Hochareon P, Manning KB, Fontaine AA, Tarbell JM, Deutsch S: Wall shear-rate estimation within the 50cc Penn State artificial heart using particle image velocimetry. *J Biomech Eng* 126: 430–437, 2004.
10. König CS, Clark C, Mokhtarzadeh-Dehghan MR: Investigation of unsteady flow in a model of a ventricular assist device by numerical modelling and comparison with experiment. *Med Eng Phys* 21: 53–64, 1999.
11. Avrahami I, Rosenfeld M, Raz S, Einav S: Numerical model of flow in a sac-type ventricular assist device. *Artif Organs* 30: 529–538, 2006.
12. Jeong GS, Shim EB, Ko HJ, Youn CH, Sun K, Goo Min B: Computational analysis of the three-dimensional hemodynamics of the blood sac in the twin-pulse life-support system. *J Artif Organs* 7: 174–180, 2004.
13. Phillips WM, Brighton JA, Pierce WS: Artificial heart evaluation using flow visualization techniques. *Trans Am Soc Artif Intern Organs* 18: 194–199, 201, 1972.
14. Nanna JC, Wivholm JA, Deutsch S, Manning KB: Flow field study comparing design iterations of a 50 cc left ventricular assist device. *ASAIO J* 57: 349–357, 2011.
15. Moosavi M-H, Fatouraee N, Katoozian H: Finite element analysis of blood flow characteristics in a Ventricular Assist Device (VAD). *Simul Model Pract Th* 17: 654–663, 2009.
16. Robbins RC, Kown MH, Portner PM, Oyer PE: The totally implantable novacor left ventricular assist system. *Ann Thorac Surg* 71(3 Suppl): S162–S165, discussion S183, 2001.
17. McDonald DA: Blood flow in arteries. *Am J Med Sci* 245: 154, 1963.
18. Van Steenhoven A, Van Dongen M: Model studies of the closing behaviour of the aortic valve. *J Fluid Mech* 90: 21–32, 1979.
19. Shi Y, Korakianitis T, Bowles C: Numerical simulation of cardiovascular dynamics with different types of VAD assistance. *J Biomech* 40: 2919–2933, 2007.
20. Guyton AC, Hall JE: *Textbook of Medical Physiology*. Philadelphia, PA, Saunders, 1991.